J Infrared Milli Terahz Waves (2012) 33:745–755
DOI 10.1007/s10762-012-9890-1

Application of Continuously Frequency-Tunable 0.4 THz Gyrotron to Dynamic Nuclear Polarization for 600 MHz Solid-State NMR

Yoh Matsuki · Keisuke Ueda · Toshitaka Idehara · Ryosuke Ikeda · Kosuke Kosuga · Isamu Ogawa · Shinji Nakamura · Mitsuru Toda · Takahiro Anai · Toshimichi Fujiwara

Received: 11 November 2011 / Accepted: 9 March 2012 /
Published online: 23 March 2012

Abstract In this paper we present results that demonstrate the utility of a continuously frequency-tunable 0.4 THz-gyrotron in a dynamic nuclear polarization (DNP)-enhanced solid-state NMR (SSNMR) spectroscopy at one of the highest magnetic fields, B_0=14.1 T (600 MHz for ^{1}H Larmor frequency). Our gyrotron called FU CW VI generates sub-mm wave at a frequency near 0.4 THz with an output power of 4–25 W and a tunability over a range of more than 1 GHz by sweeping the magnetic field at the gyrotron cavity. We observed overall down shifting of the central frequency by up to ~1 GHz at high radiation duty factors and beam current, presumably due to the cavity thermal expansion by a heating, but the tunable range was not significantly changed. The frequency tunability facilitated the optimization of the DNP resonance condition without time-consuming field-sweep of the high-resolution NMR magnet, and enabled us to observe substantial enhancement of the SSNMR signal (ε_{DNP}=12 at 90 K).

Keywords Gyrotron · Dynamic nuclear polarization · Solid-state NMR · High-field spectroscopy

1 Introduction

High-resolution solid-state nuclear magnetic resonance spectroscopy (SSNMR) is uniquely suited to studying atomic-resolution structure of insoluble or non-crystalline molecular

Y. Matsuki · K. Ueda · T. Fujiwara (✉)
Institute for Protein Research, Osaka University, 3-2 Yamadaoka Suita, Osaka 565-0871, Japan
e-mail: tfjwr@protein.osaka-u.ac.jp

T. Idehara · R. Ikeda · K. Kosuga · I. Ogawa
Research Center for Development of Far-Infrared Region, University of Fukui, Bunkyo 3-9-1, Fukui 910-8507, Japan

S. Nakamura · M. Toda · T. Anai
JEOL RESONANCE, 3-1-2 Musashino Akishima, Tokyo 196-8558, Japan

systems, such as pathogenic amyloid fibrils [1–5], physiologically important membrane proteins [6–9], and surfaces of composite materials [10, 11]. These sample systems are not amenable to other major structural analysis tools such as X-ray crystallography and solution-state NMR. Although the SSNMR is rapidly maturing, its low intrinsic sensitivity still remains the major bottleneck in many studies using SSNMR. Dynamic nuclear polarization (DNP) enhances the nuclear polarization, hence the spectral sensitivity, by coupling the large thermal equilibrium electron polarization to the nuclear spin of interest. The nuclear hyper-polarization is achieved by irradiating the electron spin resonance of a radical agent dissolved in a sample at low concentration. Together with the advancements of the millimeter- and sub-millimeter wave technologies [12–14], and the development of biradical polarizing agents [15–17], the SSNMR sensitivity enhancement of the order of 100 is routinely available via DNP. DNP has been applied to a variety of samples, ranging from small organic molecules [18, 19] and biological macromolecules [7, 20–22] to inorganic materials surfaces [10, 11].

The use of a gyrotron as a radiation source with sufficient power and long-term stability has enabled the breakthrough of the first "high-filed" DNP experiment at B_0=5 T two decades ago [23], where B_0 is the static magnetic field for NMR. With its unique ability to produce high frequency radiation at high power, the gyrotron has proved to be the most suitable source for the current CW DNP SSNMR measurements. So far, DNP-SSNMR has already been conducted at B_0<9.4 T (^{1}H frequency of 400 MHz) using millimeter waves of frequency ν<263 GHz. However, modern SSNMR spectroscopy targeting large and complex molecular systems often needs much higher fields in order to take advantage of the higher spectral separation and the sensitivity of NMR at high fields. Thus, one of the most important developments of the gyrotron has been the increase in the oscillation frequency. Based on this need, we recently constructed a high-frequency gyrotron, FU CW II producing a 395-GHz wave, and applied it to 600-MHz DNP-SSNMR experiments [24]. Terahertz (THz) wave sources at 660 GHz is required for the currently highest field high-resolution NMR performed at B_0=23.5 T (^{1}H frequency of 1 GHz).

In this work, we highlight a new degree of flexibility of the state-of-the-art gyrotrons, namely the continuous frequency tunability. In order to maximize the DNP efficiency, electron spins need to be saturated at the specific resonance condition determined by the electron and the nuclear Zeeman splittings. The optimal condition can be searched for by changing either the static magnetic field for NMR, or the frequency of the THz wave. The field/frequency-dependence of a NMR signal enhancement by DNP exhibits positive and negative maxima, where the separation for the maxima is less than or equal to twice the nuclear Zeeman splitting [25]. Therefore, it is desireable that the frequency/field can be adjusted in a range greater than the nuclear Zeeman splitting, ν_{NZ} in frequency, or B_{NZ} in magnetic field, respectively. The splitting amonts to (ν_{NZ}, B_{NZ}) = (0.6 GHz, 21 mT) for ^{1}H, and (0.15 GHz, 5 mT) for ^{13}C at B_0= 14 T. The separation of the enhancement maxima depends on the corresponding nuclear species, on the radical compounds and their concentration. Thus it is important to optimize the DNP resonance condition for each sample system.

Although THz gyrotrons with frequency step tunability (with steps of a few GHz) have been developed for years [26–28], such tunability is not appropriate for optimization of the DNP, which requires a continuous tuning. Therefore, it has been customary to optimize DNP by sweeping the magnetic field for NMR [16, 24, 29]. The field sweep, however, has several drawbacks especially when the high-field DNP for high-resolution NMR is concerned: 1) The field-sweep by changing the current of the main coil, or by using an auxiliary field sweep coil generally disturbs both the homogeneity and the stability of the field required for high-resolution NMR. 2) A tuning of the RF circuits for all relevant nuclei is required every time

when the field is adjusted. 3) It is generally difficult to construct magnets with a sweep coil at very high fields, while preserving a high resolution and the bore size. Also, it should be noted that the required sweep width increases with the field strength for the NMR. 4) A field sweep could be expensive since a large amount of liquid helium is evaporated during the sweep.

In order to solve all these issues a continuously tunable sub-THz gyrotron is necessary. The proposed design specifications for such novel radiation source include: 1) Continuous tunability over the frequency range of about twice the ^{1}H Zeeman splitting ν_{NZ} at the electron spin resonance frequency. 2) CW oscillation with high output power (>10 W) for saturating the electron spin resonance. 3) Constant output power over the frequency range. 4) Stable frequency and output power for days to a week for multi-dimensional NMR experiments. The instability should be less than 0.1 ν_{NZ} in the frequency and 1 % in the output power.

In this work, we demonstrate the aplicability of a recently developed [13] continuously frequency-tunable 0.4 THz gyrotron (FU CW VI) to DNP SSNMR experiments at a magnetic field of B_0=14.1 T (600 MHz for ^{1}H frequency), which is the highest value currently. The gyrotron is operated at the fundamental resonance mode to ensure a wide tunability (> 1 GHz) around the central frequency of about 0.4 THz, and sufficient output power (> 4 W). The frequency tunability enabled us to perform a quick and easy optimization of the DNP resonance condition while, at the same time leaving the NMR field completely undisturbed, and practically not consuming any liquid helium during the process. We will compare this *frequency*-sweeping approach with the highly time- and labor-intensive *field*-sweeping approach that we previously conducted using a fixed-frequency 0.4 THz-gyrotron (FU CW II), and sweeping the magnetic field of our high-resolution SSNMR magnet without an auxiliary sweep coil [24]. The tunable THz wave source should facilitate the retrofitting of the standard SSNMR systems for DNP without replacing the magnets, and will allow one to use various polarizing agents in a routine manner.

2 Gyrotron FU CW VI

Figure 1 shows the layout of the frequency-tunable 0.4-THz gyrotron (FU CW VI) and a 600 MHz NMR spectrometer (Vaian InfinityPlus 600) installed in adjacent rooms, together with a photograph of the gyrotron system. Our high-resolution SSNMR magnet is not equipped with an auxiliary field sweep coil. The tunability around the central frequency of 0.4 THz was achieved by using a sequence of high-order axial modes interacting with the backward wave components of the high frequency field excited in the resonator [13]. The gyrotron tube is operated at the fundamental TE_{06} mode using a 15 T cryogen-free superconducting magnet (Fig. 1a-(i)). Frequency-tunable gyrotrons operating at a similar central frequency but using the second harmonic oscillation have also been reported recently [30, 31]. The tube is being continuously evacuated by a turbo molecular pump (Fig. 1a-(ii)) to maintain the vacuum in the tube at levels of the order of 10^{-6} Pa throughout the operation. The electron beam collector and the gun coil were cooled with a chiller water circulator (Fig. 1a-(iii)). The frequency of the radiation was varied continuously by tuning the magneitc filed at the gyrotron cavity, B_{Gyro}, using a programmable power supply (Fig. 1a-(iv)). We used relatively low acceleration voltages of –12 kV on the cathode, and –7 kV on the anode, and operated magnetron injection gun (MIG) with moderate electron beam currents in the range I_b=50–150 mA. The pulsed mode radiation with a duty factor d=10–100 % was obtained using a high-voltage MOSFET switch in the cathode voltage supply line. The power supplies of the cathode (v), anode (vi) and the gun-coil (vii) were all mounted in a single 19" rack. As illustrated in Fig. 2, the beam output was

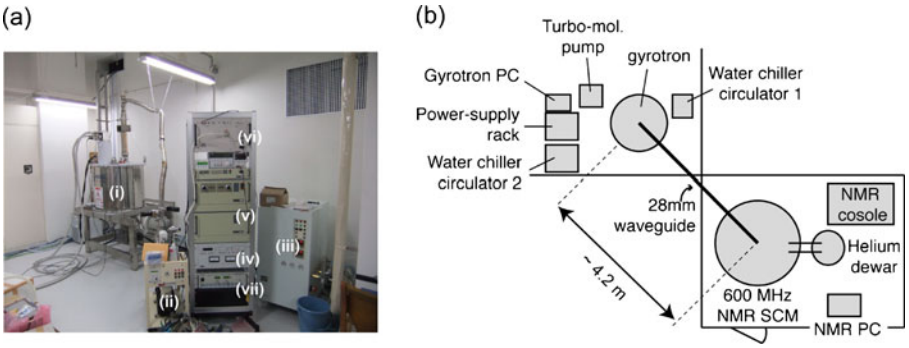

Fig. 1 (**a**) The gyrotron system installed at Institute for Protein Research, Osaka University. Helium-free 15-T SCM (i); turbo-molecular pump for the gyrotron tube (ii); pump system for water cooling of the collector of the tube and the gun coils (iii); 19" rack containing all the electric power sources for the SCM (iv), the cathode and filament (v), the anode (vi), and the gun-coils (vii). (**b**) Layout of the frequency-tunable gyrotron (FU CW VI), NMR spectrometer, and their related components.

stabilized within ±1 % using a PID feedback controll of the heater of the cathode of the MIG, taking advantage of the LABVIEW software.

The 0.4 THz-wave output from FU CW VI was directly coupled to an overmoded smooth-wall circular waveguide (made of oxygen-free copper, and having diameter of 28 mm) without any conditionning and polarization control. The wave was subsequently transmitted over 3 straight sections of the waveguide, and two miter bends to the NMR SCM, being ~4 m away from the gyrotron SCM. The waveguide was introduced from the top of the NMR SCM, going down the bore, and inputed to the NMR probe. Before the entry to the magic-angle sample spinning module, the waveguide was tapered in two steps toward the final diameter of 4 mm circular waveguide, which is terminated approximately 7 mm away from the sample rotor, and irradiates the sample transversely across the solenoidal NMR detection coil.

3 Frequency and output power

Figure 3 shows the frequency and power of the radiation from FU CW VI measured as a function of the gyrotron field, B_{Gyro}. The frequency of the radiation was measured with a heterodyne measurement system consisting of a 16th harmonic mixer (Virginia Diodes WR-

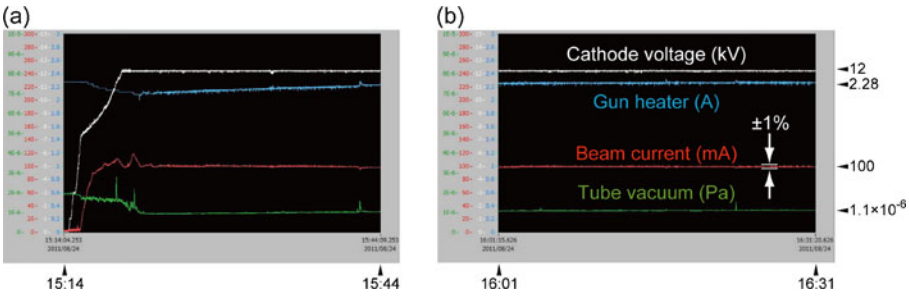

Fig. 2 LABVIEW remote interface for monitoring and controlling the gyrotron FU CW VI. Starting the gyrotron takes only about 5 min (**a**). The beam output can be stabilized to ±1 % by a PID feedback control of the filament output (**b**).

2.2HM), a spectrum analyzer (Agilent N1996A) and a signal generator (Agilent E8257D). The ouput power was measured from the temperature increase of a water load (30 ml in a quartz glass cone).

We started operating the gyrotron in a pulsed mode, then proceeded to a CW operation. In the pulsed mode operation (5 Hz, d=10 %), the frequency of the radiation was changed almost linearly from 394.4 to 395.6 GHz over the range of ~1.2 GHz along with the B_{Gyro} tuned from 14.35 and 14.55 T (Fig. 3(a), blue data). The time-averaged radiation power varied between 0.8 and 3 W for the frequency range (Fig. 3(b), blue data). The output power was high at the edges of the frequency range, at around B_{Gyro}=14.35 and 14.55 T.

In a CW operation, the frequency could be swept from 393.85 to 394.95 GHz for the range of just over 1 GHz at the beam current I_b=100 mA (Fig. 3a, red data). Interestingly, the output frequency exhibited overall down shift in the CW operations (Fig. 3(a), green and red data), as compared to the measurement in the pulsed mode (blue data). The observed shift was larger at higher beam current, namely by ~1.0 GHz and ~1.4 GHz at I_b=50 mA and 100 mA, respectively, measured at B_{Gyro}=14.475 T. The progressive down shifting observed at higher radiation duty factors and beam currents suggests a possible cavity expansion by heating. With this assumption, the frequency shifts correspond to a cavity diameter increased by ~12.0 and ~16.8 μm, respectively, or to temperature increase by 150 and 200 K based on the expansion coefficient for oxygen-free copper (16.6×10^{-6} K^{-1}).

The radiation power in CW mode varied almost monotonically from 4 to 12 W at I_b=50 mA, and from 3 to 25 W at I_b=100 mA over the frequency range from about 395 to 394 GHz (Fig. 3, green and red data). The power output was maximum at around B_{Gyro}=14.43 T–14.45 T regardless of the beam current, and decreased towards B_{Gyro}=14.6 T.

4 DNP-SSNMR experiments

The sample for DNP SSNMR measurements was a standard frozen glass-forming liquid, d_8-glycerol/D_2O/H_2O=6/3/1 (wt/wt/wt), doped with 20 mM of the biradical polarizing agent, TOTAPOL [17]. The sample was center-packed to a 3.2 mm-φ Si_3N_4 rotor using cylindrical Kel-F top and bottom spacers. The sample temperature could be precisely set between 30 K

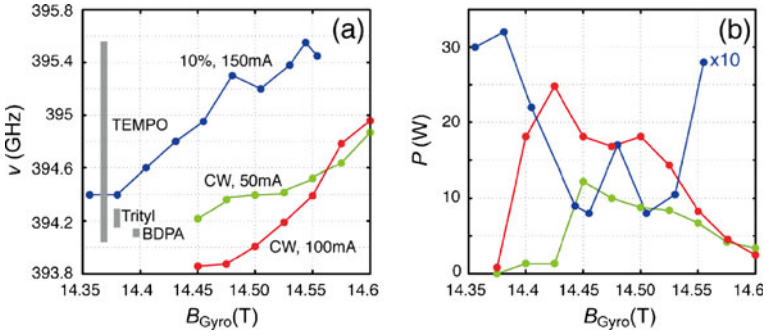

Fig. 3 The frequency (**a**) and power (**b**) of the THz wave from FU CW VI measured as a function of the gyrotron field strength, B_{Gyro} with various radiation duty factors (d) and beam currents (I_b): d=10 % (5 Hz) and I_b (peak value)=150 mA for blue data; d=100 %, i.e. CW and I_b=50 mA for green data; CW and I_b=100 mA for red data. In panel (a), the position and breadth of the EPR lines of the major DNP polarizing agents, TEMPO (and TEMPO-based multi-radicals), Trityl and BDPA, calculated for our NMR filed B_0=14.0618 T are shown with gray bars.

and 90 K using the circulation of temperature-controlled helium gas in the sample room. The ^{1}H NMR signal was observed by a direct excitation of the ^{1}H polarization with a $\pi/2$ pulse. The excitation pulse was preceded by a train of $\pi/2$ pulses for saturating the initial ^{1}H polarization, and a polarization buildup time period of 15 s. The ^{1}H DNP enhancement factor was measured as the ratio of the integral signal intensities observed with and without THz wave irradiation as $\varepsilon_{DNP}=I_{ON}/I_{OFF}$. Therefore, the enhancement factor ε_{DNP} of 1.0 indicates no NMR signal enhancement, i.e. the intensity under the THz wave irradiation is identical to that given by the thermal nuclear polarization at the same temperature. By this definition, $\varepsilon_{DNP}>1$, and <1 in this work is referred to as the "positive" and "negative" DNP enhancement, respectively. Further details on the equipments and DNP experiments at the helium temperaures will be given in a separate publication (in preparation).

4.1 DNP-SSNMR using the pulsed mode radiation

First, we characterized the utility of the tunable gyrotron using the pulsed mode radiation (5 Hz, d=10 %) in DNP SSNMR measurements. In Fig. 4 gives the ^{1}H DNP enhancement factors observed at 90 K, along with the B_{Gyro} sweep, hence the frequency sweep of the THz wave (filled circles). The NMR field was fixed at B_0=14.0618 T (598.7 MHz for the ^{1}H frequency). The positive and negative enhancements were observed in turn while the frequency of the THz wave was swept down, as expected from the theory [32]. The DNP efficiency was maximized at around B_{Gyro} =14.40 and 14.52 T, where the maximum positive and negative enhancements of ε_{DNP}=2 and −0.5, respectively, were observed. The magnitudes of the enhancements were relatively small because of the small radiation duty factor. The THz wave frequencies giving the enhancement maxima were 394.52 and 395.25 GHz as seen from Fig. 3a. The frequency separation of ~0.7 GHz, which is close to the ^{1}H nuclear Zeeman splitting (~0.6 GHz), suggests that the DNP mainly occured via the cross effect (CE) [25] at B_0=14.1 T. The disappearance of the enhancement at around B_{Gyro}=14.42 and 14.50 T as indicated by arrows in Fig. 4 corresponds to the gyrotron field positions where the DNP process was inefficient due to very small output power (<0.2 W) as shown in Fig. 3(b).

Previously, we observed a similar field dependency of the DNP enhancement with a fixed-frequency gyrotron operating at ν=394.5 GHz when sweeping the NMR field.[24]

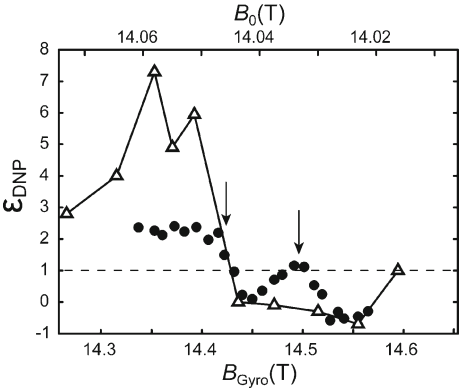

Fig. 4 ^{1}H DNP enhancement factor observed as a function of the gyrotron field strength B_{Gyro} (lower x-scale) at a fixed (B_0=14.0618 T) NMR field strength (filled circles), or as a function of the NMR field strength B_0 (upper x-scale) at a fixed (ν=394.5 GHz) THz wave frequency (open triangles). Both data were taken at 90 K. Arrows show the gyrotron fields where the output power was small as seen in Fig. 3(b).

The enhancement factors observed for the fixed-frequency gyrotron are reproduced in Fig. 4 with open triangles as a function of the NMR filed strength, B_0. This field sweep experiment was conducted by changing the main coil current of the NMR SCM since the required field strength for the sweep was not attainable by the Z_0 shim coil for our magnet. The acquisition of ten data points (open triangles) with the field-sweep approach took more than 24 hours, or three full working days of eight hours each. In contrast, in the frequency-sweep measurement using the tunable gyrotron, we obtained 25 data points shown in Fig. 4 (filled circles) in less then 1 h. For each data point, two identical measurements were conducted, and the calculated enhancements were averaged: total 50 NMR spectra were recorded for the trace. Thus, the frequency-sweep approach enabled about 100-fold faster data collection (50 spectra in 1 h vs 10 spectra in 24 h) than the field-sweep approach in the DNP optimization.

The frequency-sweeping approach is not only faster but also easier and less expensive. The SCM of the gyrotron can be mainteined in a driven-mode, and easily controlled with a programmable power supply. This is allowed because only relatively low field homogeneity (~10^{-2}%) is enough at the gyrotron cavity, and the size of the homogeneous region around the cavity (~100 mm^2) is small. In contrast, high-resolution NMR SCM must be stabilized in the persistent current mode and carefully optimized for gaining the very high field homogeneity (i.e. the NMR spectral resolution) in the order of 1 ppb (~10^{-7}%), and the size of the homogeneous region required around the SSNMR sample is much larger (~1000 mm^2). Also, every time the NMR field is adjusted, the stability of the coil current is disrupted, and needs some time before the field is stabilized again. Additionally, the RF circuit for the NMR detection should be re-tuned for all relevant nuclei. The field-sweep approach can also be expensive. Our three-day field-sweep measurement evaporated ~250 L of liquid helium from the NMR SCM, while the frequency-sweep measurement consumed virtually no liquid helium since our gyrotron uses a cryogen-free magnet. If the NMR SCM is equipped with an auxiliary coil, the field sweeping would be easier than sweeping the NMR SCM directly. However, it is technically challenging to constract magnets with a sweep coil at very high fields, while preserving high resolution and the bore size. It should be also noted that the required sweep width increases with the NMR field strength due to a nuclear Zeeman splitting.

4.2 DNP-SSNMR in the CW mode

Next, we performed the DNP SSNMR experiments using the CW radiation from the frequency-tunable gyrotron. Figure 5 shows the DNP enhancement factor measured as a function of the gyrotron field, B_{Gyro}, at various radiation duty factors (pulsed mode to CW) and beam currents (I_b=50 – 100 mA) at 90 K. Better electron saturation by the CW radiation as compared to the pulsed-mode irradiation should improve the enhancement. The CW irradiation is the most efficient method for saturating the electron transition since it generates the highest time-averaged THz magnetic field for a given THz-wave power. Indeed, the maximum positive enhancements, ε_{DNP}=7±0.2 and 13±0.4, were observed with I_b=50 mA and 100 mA (green and red full lines in Fig. 5), respectively. These enhancements are more than three and six times larger than those observed in the pulsed mode. The larger enhancement at higher beam current shows that the electron polarization was not completely saturated at 7 – 9 W obtained with these beam currents around B_{Gryro}=14.55 T. In our current system, the transmission efficiency of the THz wave from the gyrotron to the sample is not optimal. With a due improvement in the transmission line, even larger enhancement is expected.

Besides the efficiency of the electron saturation, we observed that higher radiation duty factors and beam currents decreased the frequency of the radiation (Fig. 3a), due to the putative thermal expansion of the gyrotron cavity. Notably, the frequency range obtained in

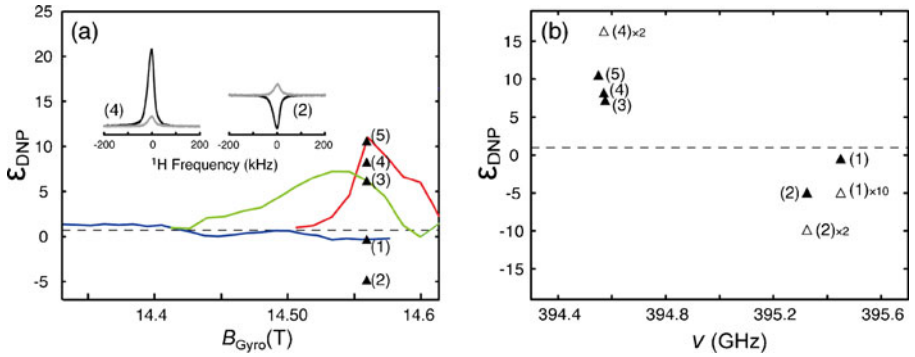

Fig. 5 (**a**) ^{1}H DNP enhancement as a function of the gyrotron field, B_{Gyor}, observed at various radiation duty factors and beam currents. The data are plotted with the same color code for the radiation duty factors and beam currents as in Fig. 3. The blue line shows the same enhancement data as given in Fig. 4 with filled circles. All data were recorded at 90 K. The enhancements indicated with filled triangles were measured at a fixed gyrotron field B_{Gyro}=14.56 T, but as a function of the radiation duty factor (d) and the beam current (I_{b}): (1) d=10 %, I_{b}=150 mA; (2) d=50 %, I_{b}=40 mA; (3) d=100 %, i.e. CW, I_{b}=50 mA; (4) d=50 %, I_{b}=120 mA; (5) CW, I_{b}=100 mA. Two representative ^{1}H NMR spectra recorded at conditions (2) and (4) are shown in the inset. The gray spectra were obtained without a THz wave irradiation, showing the signal obtained for the thermal nuclear polarization at 90 K. (**b**) The same data points as shown in (a) with filled triangles plotted as a function of the corresponding THz wave frequency that can be seen in Fig. 3(a). For combinations of the radiation duty factor and the beam current, for which the frequency measurement was not conducted, the frequency was estimated by interpolating observed frequencies by assuming that the product of the duty factor and the beam current, $d\times I_{\mathrm{b}}$, is proportional to the heat at the cavity, thus to the frequency shift due to the cavity expansion. The data points shown in open triangles show the enhancement factor scaled by the inverse of the radiation duty factor by assuming that the enhancement linearly depends on the incident THz wave power being far from the complete electron saturation.

the CW mode covered only the low frequency half of the EPR line of TEMPO or TEMPO-based biradicals (green and red lines in Fig. 3a). Because of this, we observed a series of positive enhancements with the B_{Gyro} sweep (green and red lines in Fig. 5a), rather than the transition from the negative to positive enhancements seen for the pulsed mode radiation (blue line in Fig. 5a). Also being consistent with the lower frequency radiation range obtained at a higher beam current, the profile of the B_{Gryro}-dependence of the enhancement obtained at I_{b}=100 mA (Fig. 5a, red lines) appeared narrower than that at I_{b}=50 mA (green line).

The data points shown with filled triangles in Fig. 5(a) were recorded at a fixed gyrotron field B_0=14.56 T for the various radiation duty factor (d) and beam current (I_{b}). The observed dependence of the sign and the magnitude of the DNP enhancements illustrates the concomitant effects of the electron saturation efficiency and the frequency shift of the radiation. At a small radiation duty (d=10 %), a weak negative DNP enhancement was observed at a relatively high beam current, I_{b}=150 mA (Fig. 5(1): $d\times I_{\mathrm{b}}$=15). With a higher duty (d=50 %) and a lower beam current (I_{b}=40 mA), the magnitude of the enhancement was increased at the frequency still in the range that gives rise to a negative enhancement, ((2): $d\times I_{\mathrm{b}}$=20). At a higher duty factor (d=100 %, i.e. CW) and a similar beam current, the enhancement was inverted to yield a positive enhancement factor, ((3): $d\times I_{\mathrm{b}}$=50). A positive enhancement in a simlar magnitude was observed with a very high beam current (I_{b}=120 mA) when the duty is low (d=50 %), ((4): $d\times I_{\mathrm{b}}$=60). With the high duty (CW) and a high beam current (I_{b}=100 mA), the largest positive enhancement was observed at 90 K, ((5): $d\times I_{\mathrm{b}}$=100). In the inset, two representative ^{1}H NMR spectra obtained at the conditions (2) and (4) are shown as a superposition of the spectra recorded with (black) and without (gray) THz wave irradiation.

In Fig. 5(b), the same data points as shown with filled triangles in panel (a) are plotted as a function of the THz wave frequency. This illustrates that the range of the radiation duty and the beam current employed changed the radiation frequency by up to ~0.9 GHz at B_{Gyro}=14.56 T, resulting in negative and positive enhancements. When the enhancements obtained in the pulsed mode (d<100 %) were scaled by the inverse of the radiation duty factor on an assumption that the enhancement linearly depends on the incident THz wave power for weak radiation (open triangles), the positive and negative enhancement maxima exhibited a similar magnitude of ~10 at 90 K. The frequency yielding the enhancement maxima were separated by roughly 0.6 GHz, corresponding to the nuclear Zeemann splitting, again confirming the DNP via CE mechanism.

5 Conclusions

In Introduction, we specified the key requirements for the THz wave sources for DNP SSNMR under high field conditions. Particularly, we highlighted the continuous frequency tunability of the THz gyrotron FU CW VI, and demonstrated its utility in the optimization of the DNP conditions at one of the highest field values B_0=14.1 T. We summarize our results comparing them with the targeted specifications:

1) The gyrotron FU CW VI was continuously frequency-tunable over a range of>1 GHz, i.e., ~$2\nu_{NZ}$ for ^{1}H, at the central frequency of about 395 GHz by sweeping the magnetic field at the cavity of the gyrotron. The frequency range obtained for the CW radiation at a high-beam current included the condition for the maximum positive enhancement, thus allowed a quick and easy optimization of the DNP efficiency. In addition, as shown with gray bars in Fig. 3a, the frequency range contained the EPR frequencies of several major radical compounds (TEMPO and its derivatives, trityl and BDPA) that have been used in DNP SSNMR experiments. Therefore, this tunability will facilitate serial expeiments for samples doped with different polarizing agents.
2) The output power was not constant over the frequency range. The output power varied gradually in a range 4 - 25 W for the CW radiation at I_b=100 mA (Fig. 3). This output power, however, was sufficient to enhance the SSNMR signal (ε_{DNP}=12 at 90 K). Although this power variation was not a problem in maximizing the sensitivity enhancement, a quantitative analysis of the frequency profile of the DNP enhancement may be hampered. An analyisis of the profile under the experimental conditions such as sample temperature, THz wave power, and molecular structure of the radical agent should elucidate the DNP process quantitatively. The frequency dependent modulation of the output power can be reduced by controlling the beam current, or by using a variable attenuator. Since the output power of at least ~4 W at B_{Gyro}=14.575 T was enough for the signal enhancement, this simple approach should suffice to assure an accuracy for the enhancement profile.
3) The gyrotron frequency and the output power were stable within about 0.1 GHz and 1 %, respectively, over a day. Although we observed down shifting of the frequency by up to ~1 GHz at high radiation duty factors and beam currents, presumably due to the cavity expansion caused by heating, this did not affect the stability. The frequency of the radiation was reproducible for a given beam current and radiation duty. The tunability range was not changed significantly.

The DNP optimization has been performed so far by sweeping the magnetic field for NMR. The frequency tunability greatly facilitated the optimization of DNP since the time-consuming

field sweep of the high-resolution NMR magnet and tuning of the RF circuit for NMR were unnecessary. The gyrotron tunability allows a routine optimization of the DNP for various radical polarizing agents and nuclear species, thus expands the applicability of DNP-NMR experiments. The application of a continuously tunable gyrotron will also facilitate the upgrading of the standard SSNMR spectrometers with the DNP hyperpolarization capability without modifying the NMR magnet. The increased accessibility to the DNP sensitivity enhancement should benefit a wide range of studies using a SSNMR spectroscopy. It is expected that the constant growth of the THz wave technologies will provide more compact and inexpensive tunable gyrotron, which can be used as a standard component of the equipment for the next generation of DNP SSNMR systems.

Acknowledgment This research is partly supported by SENTAN, JST and Targeted Proteins Research Program, MEXT.

References

1. G. T. Debelouchina, M. J. Bayro, P. C. van der Wel, M. A. Caporini, A. B. Barnes, M. Rosay, W. E. Maas, R. G. Griffin, *Phys Chem Chem Phys*, ***12***, 5911 (2010).
2. G. T. Debelouchina, G. W. Platt, M. J. Bayro, S. E. Radford, R. G. Griffin, *J Am Chem Soc*, ***132***, 17077 (2010).
3. K. Iwata, T. Fujiwara, Y. Matsuki, H. Akutsu, S. Takahashi, H. Naiki, Y. Goto, *Proc. Natl. Acad. Sci. USA*, ***103***, 18119 (2006).
4. A. K. Paravastu, R. D. Leapman, W.-M. Yau, R. Tycko, *Proc. Natl. Acad. Sci. USA*, ***105***, 18349 (2008).
5. C. Wasmer, A. Lange, H. Van Melckebeke, A. B. Siemer, R. Riek, B. H. Meier, *Science*, ***319***, 1523 (2008).
6. C. Ader, R. Schneider, S. Hornig, P. Velisetty, E. M. Wilson, A. Lange, K. Giller, I. Ohmert, M. F. Martin-Eauclaire, D. Trauner, S. Becker, O. Pongs, M. Baldus, *Nat Struct Mol Biol*, ***15***, 605 (2008).
7. V. S. Bajaj, M. L. Mak-Jurkauskas, M. Belenky, J. Herzfeld, R. G. Griffin, *Proc. Natl Acad Sci USA*, ***106***, 9244 (2009).
8. M. Etzkorn, S. Martell, O. C. Andronesi, K. Seidel, M. Engelhard, M. Baldus, *Angew. Chem. Int. Ed.*, ***46***, 459 (2007).
9. M. E. Ward, L. Shi, E. Lake, S. Krishnamurthy, H. Hutchins, L. S. Brown, V. Ladizhansky, *J Am Chem Soc*, ***133***, 17434 (2011).
10. M. Lelli, D. Gajan, A. Lesage, M. A. Caporini, V. Vitzthum, P. Mieville, F. Heroguel, F. Rascon, A. Roussey, C. Thieuleux, M. Boualleg, L. Veyre, G. Bodenhausen, C. Coperet, L. Emsley, *J Am Chem Soc*, ***133***, 2104 (2011).
11. A. Zagdoun, A. J. Rossini, D. Gajan, A. Bourdolle, O. Ouari, M. Rosay, W. E. Maas, P. Tordo, M. Lelli, L. Emsley, A. Lesage, C. Coperet, *Chem Commun (Camb)*, in press. (2011).
12. V. S. Bajaj, M. K. Hornstein, K. E. Kreischer, J. R. Sirigiri, P. P. Woskov, M. L. Mak-Jurkauskas, J. Herzfeld, R. J. Temkin, R. G. Griffin, *J. Magn. Reson.*, ***189***, 251 (2007).
13. T. Idehara, K. Kosuga, L. Agusu, R. Ikeda, I. Ogawa, T. Saito, Y. Matsuki, K. Ueda, T. Fujiwara, *J Infrared Millim Teraherz.*, ***31***, 775 (2010).
14. E. A. Nanni, A. B. Barnes, R. G. Griffin, R. J. Temkin, *IEEE Trans. Teraherz. Tech.*, ***1***, 145 (2011).
15. K. N. Hu, *Solid State Nucl Mag*, ***40***, 31 (2011).
16. Y. Matsuki, T. Maly, O. Ouari, H. Karoui, F. Le Moigne, E. Rizzato, S. Lyubenova, J. Herzfeld, T. Prisner, P. Tordo, R. G. Griffin, *Angew Chem Int Ed*, ***48***, 4996 (2009).
17. C. S. Song, K. N. Hu, C. G. Joo, T. M. Swager, R. G. Griffin, *J Am Chem Soc*, ***128***, 11385 (2006).
18. C. G. Joo, A. Casey, C. J. Turner, R. G. Griffin, *J Am Chem Soc*, ***131***, 12 (2009).
19. V. Vitzthum, M. A. Caporini, G. Bodenhausen, *J. Magn. Reson.*, ***205***, 177 (2010).
20. U. Akbey, W. T. Franks, A. Linden, S. Lange, R. G. Griffin, B. J. van Rossum, H. Oschkinat, *Angew Chem Int Ed*, ***49***, 7803 (2010).
21. A. B. Barnes, B. Corzilius, M. L. Mak-Jurkauskas, L. B. Andreas, V. S. Bajaj, Y. Matsuki, M. L. Belenky, J. Lugtenburg, J. R. Sirigiri, R. J. Temkin, J. Herzfeld, R. G. Griffin, *Phys Chem Chem Phys*, ***12***, 5861 (2010).
22. M. J. Bayro, G. T. Debelouchina, M. T. Eddy, N. R. Birkett, C. E. MacPhee, M. Rosay, W. E. Maas, C. M. Dobson, R. G. Griffin, *J Am Chem Soc*, ***133***, 13967 (2011).

23. L. R. Becerra, G. J. Gerfen, R. J. Temkin, D. J. Singel, R. G. Griffin, *Phys Rev Lett*, ***71***, 3561 (1993).
24. Y. Matsuki, H. Takahashi, K. Ueda, T. Idehara, I. Ogawa, M. Toda, H. Akutsu, T. Fujiwara, *Phys Chem Chem Phys*, ***12***, 5799 (2010).
25. T. Maly, G. T. Debelouchina, V. S. Bajaj, K. N. Hu, C. G. Joo, M. L. Mak-Jurkauskas, J. R. Sirigiri, P. C. A. van der Wel, J. Herzfeld, R. J. Temkin, R. G. Griffin, *J Chem Phys*, ***128***, 052211 (2008).
26. K. D. Hong, G. F. Brand, T. Idehara, *J Appl Phys*, ***74***, 5250 (1993).
27. T. Idehara, I. Ogawa, S. Mitsudo, M. Pereyaslavets, N. Nishida, K. Yoshida, *IEEE Trans. Plasma Sci*, ***27***, 340 (1999).
28. T. Idehara, T. Tatsukawa, H. Tanabe, S. Matsumoto, K. Kunieda, K. Hemmi, T. Kanemaki, *Phys Fluids B-Plasma*, ***3***, 1766 (1991).
29. M. Rosay, L. Tometich, S. Pawsey, R. Bader, R. Schauwecker, M. Blank, P. M. Borchard, S. R. Cauffman, K. L. Felch, R. T. Weber, R. J. Temkin, R. G. Griffin, W. E. Maas, *Phys Chem Chem Phys*, ***12***, 5850 (2010).
30. M. K. Hornstein, V. S. Bajaj, R. G. Griffin, R. J. Temkin, *IEEE Trans Plasma Sci IEEE Nucl Plasma Sci Soc*, ***34***, 524 (2006).
31. A. C. Torrezan, S. T. Han, I. Mastovsky, M. A. Shapiro, J. R. Sirigiri, R. J. Temkin, A. B. Barnes, R. G. Griffin, *IEEE Trans Plasma Sci IEEE Nucl Plasma Sci Soc*, ***38***, 1150 (2010).
32. K. N. Hu, G. T. Debelouchina, A. A. Smith, R. G. Griffin, *J Chem Phys*, ***134***, 125105 (2011).